axioms

MDPI

Article

A One-Phase Fractional Spatial Stefan Problem with Convective Specification at the Fixed Boundary

Diego E. Guevara [1,2], Sabrina D. Roscani [1,3,*], Domingo A. Tarzia [1,3] and Lucas D. Venturato [1,3]

[1] Consejo Nacional de Investigaciones Científicas y Técnicas (CONICET), Buenos Aires C1425FQB, Argentina; dguevara@fceia.unr.edu.ar (D.E.G.); dtarzia@austral.edu.ar (D.A.T.); lventurato@austral.edu.ar (L.D.V.)
[2] Departamento de Matemática, Escuela de Ciencias Exacta y Naturales, Facultad de Ciencias Exactas, Ingeniería y Agrimensura, Universidad Nacional de Rosario, Rosario S2000FZF, Argentina
[3] Departamento de Matemática, Facultad de Ciencias Empresariales, Universidad Austral, Paraguay 1950, Rosario S2000FZF, Argentina
* Correspondence: sroscani@austral.edu.ar

Abstract

We address a fractional spatial Stefan problem derived from a non-Fourier heat flux model with a convective boundary condition at the fixed boundary. An explicit solution is obtained in terms of a three-parameter Mittag–Leffler function. A dimensionless formulation is used to derive a family of fractional spatial Stefan problems that depend on the Biot and Stefan numbers. Finally, a straightforward numerical method for approximating the solutions is presented, along with numerical experiments analyzing the influence of the physical parameters and the order of fractional differentiation.

Keywords: fractional Stefan problem; Caputo flux; Robin condition

MSC: 26A33; 35C06; 80A22

Academic Editor: Ricardo Almeida

Received: 27 August 2025
Revised: 1 October 2025
Accepted: 5 October 2025
Published: 8 October 2025

Citation: Guevara, D.E.; Roscani, S.D.; Tarzia, D.A.; Venturato, L.D. A One-Phase Fractional Spatial Stefan Problem with Convective Specification at the Fixed Boundary. *Axioms* **2025**, *14*, 757. https://doi.org/10.3390/axioms14100757

1. Introduction

Fractional Stefan problems constitute a broad field that addresses free boundary problems of the Stefan type using fractional operators (e.g., fractional Laplacian [1], Riesz, or Caputo derivatives [2]). These operators can be applied in the time or space variables, generating different models. When applied in the temporal domain, they are associated with memory effects, whereas when applied in the spatial domain, they describe nonlocal phenomena. Such anomalous behaviors are often linked to the heterogeneity of the materials or media being analyzed, as can be observed in [3–9].

In this article, we deal with a fractional variant of the classical one-dimensional, one-phase Stefan problem with a convective-type boundary condition. The fractional model is derived from the assumption of a nonlocal heat flux expressed in terms of a Caputo derivative. That is

$$q(x,t) = \begin{cases} -k_\alpha \, {}_0^C D_x^\alpha u(x,t) & \text{for } x < s(t) \quad \text{(Liquid)} \\ 0 & \text{for } s(t) < x \quad \text{(Solid)} \end{cases}$$

where k_α is a constant introduced to maintain dimensional consistency, and thus we will focus on a problem governed by a space-fractional diffusion equation. Examples in the literature of spatial nonlocality include dendritic crystal growth [10], scaled Brownian motion [11], and water infiltration in heterogeneous underground soils [12].

A fundamental distinction between classical and fractional one-dimensional Stefan problems lies in the evolution of the free boundary. As shown in [13–15], in the case of fractional Stefan problems with a constant temperature prescribed at the fixed boundary, the corresponding self-similar solutions reveal that the free boundary evolves proportionally to $t^{1/1+\alpha}$ (superdiffusion) or to $t^{\alpha/2}$ (subdiffusion), instead of the classical diffusion case, where the advance of the interface is proportional to $\sqrt{t}$. The same behavior has been observed for quasi-stationary fractional problems [2].

In this work, we obtain an explicit self-similar solution to the one-dimensional fractional Stefan problem with a convective-type boundary condition. By employing a self-similar transformation, we reduce the governing partial differential equation to a fractional ordinary differential equation, which allows for an analytical characterization of the free boundary evolution. Furthermore, we introduce the corresponding dimensionless problem, which is characterized by two physical parameters, the Stefan number (Ste) and the Biot number (Bi). Through systematic variation of these parameters, we examine the behavior of the fractional model and compare it with the classical Stefan problem. This analysis is particularly relevant given that convective boundary conditions are among the most frequently encountered in natural and engineering contexts. Our findings support the suitability of the fractional model to describe a free boundary process involving anomalous diffusion of nonlocal type, where the advance of the free boundary is a superdiffusive phenomenon. To facilitate future implementations and applications of the model, we developed an analytical–numerical simulation of the self-similar solution using an explicit scheme in `Python`. This computational framework allows for the reproduction of the solution under various configurations of the physical parameters, offering a practical tool for exploring the implementation of a superdiffusion model with convective boundary conditions in a phase-change process. The full codebase, along with usage examples and documentation, is openly available on GitHub at https://github.com/degarch/Stefan_problem (accessed on 4 October 2025) and has been archived on Zenodo [16].

2. The Non-Fourier Caputo Model

Before proceeding with the full formulation of the model, we introduce a generalization of Fourier's law that allows for the incorporation of possible anomalous diffusion behavior. This generalization is based on fractional operators in the Caputo sense, leading to what is known as the non-Fourier Caputo model. With the aim of completeness, we present the definitions of the fractional operators involved in our model.

Definition 1. *Let $-\infty < a < b < \infty$ and $\alpha \in (0,1)$. The Riemann–Liouville fractional integral of order α is defined for each $f \in L^1(a,b)$ as*

$$ {}_aI^{\alpha} f(x) = \frac{1}{\Gamma(\alpha)} \int_a^x (x-p)^{\alpha-1} f(p)\, \mathrm{d}p. $$

Definition 2. *Let $\alpha \in (0,1)$ and $f \in AC[a,b]$. The Riemann–Liouville fractional derivative of order α is defined for $x > a$ as*

$$ {}^{RL}_{a}D^{\alpha} f(x) = \frac{1}{\Gamma(1-\alpha)} \frac{d}{dx} \int_a^x (x-p)^{-\alpha} f(p)\, \mathrm{d}p, $$

and the Caputo fractional derivative of order α is defined for $x > a$ as

$$ {}^{C}_{a}D^{\alpha} f(x) = \frac{1}{\Gamma(1-\alpha)} \int_a^x (x-p)^{-\alpha} \frac{d}{dx} f(p)\, \mathrm{d}p. $$

2.1. Governing Equations

Consider a cylindrical domain Ω with a constant cross-sectional area A and length $[0, l]$, where $l \gg 1$, composed of a phase-change material exhibiting anomalous diffusion. Let $u = u(x,t)$ denote the temperature of the slab at position x and time t, and let $q = q(x,t)$ denote the associated heat flux, assuming that the lateral surface and the end at $x = l$ of the bar are thermally insulated.

We suppose that, initially, the bar is at its melting temperature $u = U_m$ and that a sharp-interface-type melting process begins by imposing a temperature flux at the fixed face $x = 0$. According to the sharp interface hypothesis, we can identify the free boundary s as a function of time, $s = s(t)$, which represents the position of the melting front at each instant $t > 0$. Moreover, we consider s to be an increasing function $x = s(t)$ with inverse $t = h(x)$.

In this way, for later times $t > 0$, a sharp interface located at $x = s(t)$ separates the liquid phase, with temperature $u > U_m$ to the left of $s(t)$, from the solid phase, which remains at a constant temperature $u = U_m$ to the right of $s(t)$; the interface moves from left to right as time increases.

The total energy of the model is given by the enthalpy, denoted as e. Since, by our assumptions, e is zero in the solid region and is characterized by the sum of sensible and latent heat in the liquid region, the enthalpy per unit mass is given as follows:

$$e(x,t) = \begin{cases} \ell + c(u(x,t) - U_m) & \text{for } x < s(t) \quad \text{(Liquid)} \\ 0 & \text{for } s(t) < x \quad \text{(Solid)}, \end{cases} \tag{1}$$

where ℓ is the latent heat energy per unit mass and c is the sensible heat capacity of the liquid phase. Now, unlike the classical model, our heat flux q will not be described by Fourier's law, but rather by a fractional heat flux. More specifically,

$$q(x,t) = \begin{cases} \dfrac{-k_\alpha}{\Gamma(1-\alpha)} \displaystyle\int_0^x (x-p)^{-\alpha} \frac{\partial}{\partial p} u(p,t) \mathrm{d}p & \text{for } x < s(t) \quad \text{(Liquid)} \\ 0 & \text{for } s(t) < x \quad \text{(Solid)} \end{cases} \tag{2}$$

or, in terms of fractional derivatives,

$$q(x,t) = \begin{cases} -k_\alpha \, {}_0^{\mathrm{C}}D_x^\alpha u(x,t) & \text{for } x < s(t) \quad \text{(Liquid)} \\ 0 & \text{for } s(t) < x \quad \text{(Solid)} \end{cases} \tag{3}$$

where $k_\alpha = \nu_\alpha k$, k is the thermal conductivity, $[\nu_\alpha] = [L^{\alpha-1}]$ is a constant introduced to maintain dimensional consistency, and $[L]$ is a generic unit of length (we refer to Table 1 for complete nomenclature information).

The non-Fourier heat flux (3) reflects the nonlocal nature of the fractional derivative, meaning that the flux at a given point x depends on the temperature gradient over the entire region to the left of x. In particular, the Caputo-type formulation incorporates a weighted contribution of the temperature gradients at all points to the left of x, with the weights given by a power-law kernel $(x-p)^{-\alpha}$. This formulation is intended to capture anomalous diffusion effects observed in certain complex media. The zero-flux condition in the solid region simply reflects the fact that this part remains at a constant temperature and no heat propagation occurs beyond the free boundary $s(t)$.

Let us now derive the governing equations. The first law of thermodynamics states that the change in internal energy, denoted by ΔE, in a given system is equal to the total energy supplied, which includes the heat added to the system, Q, with no mechanical work. This relationship is expressed as

$$\Delta E = Q. \tag{4}$$

Table 1. Nomenclature table with property dimensions: $[M]$ mass, $[T]$ time, $[L]$ length, and $[\Theta]$ temperature.

Symbol	Definition	Dimension
u	Temperature	$[\Theta]$
x	Spatial position	$[L]$
t	Time	$[T]$
k	Thermal conductivity	$[\frac{ML}{T^3\Theta}]$
ρ	Mass density	$[\frac{M}{L^3}]$
c	Specific heat	$[\frac{L^2}{T^2\Theta}]$
$d = \dfrac{k}{\rho c}$	Diffusion coefficient	$[\frac{L^2}{T}]$
ℓ	Latent heat per unit mass	$[\frac{L^2}{T^2}]$
h	Heat transfer coefficient	$[\frac{M}{T^3\Theta}]$
μ_α	Temporal constant for dimensional consistency	$\left[T^{\frac{\alpha}{1+\alpha}}\right]$
ν_α	Spatial constant for dimensional consistency	$\left[L^{\alpha-1}\right]$
U_m	Phase change temperature	$[\Theta]$
U_∞	Ambient temperature	$[\Theta]$
$\mathrm{Ste} = \dfrac{c\,(U_\infty - U_m)}{\ell}$	Stefan number	$[-]$
$\mathrm{Bi} = \dfrac{x_0 h}{k}$	Biot number	$[-]$

Moreover, since there are no pressure changes in the system, the variation in internal energy depends entirely on the volumetric enthalpy, defined as the product of the density ρ and the specific enthalpy function e given in (1). Therefore, the variation in internal energy within the volume over the time interval $[0, t]$ can be expressed as

$$\Delta E = \int_\Omega \rho[e(x,t) - e(x,0)]\,\mathrm{d}V \tag{5}$$

and the heat supplied in this time interval as

$$Q = \int_0^t \int_{\partial\Omega} q(x,\tau)\mathrm{d}S + \int_0^t \int_\Omega f(x,t)\mathrm{d}V, \tag{6}$$

where $\partial\Omega$ denotes the boundary of the domain Ω through which heat enters or leaves the system and f represents an external source. By substituting Equations (5) and (6) into the expression of the first law (4) and assuming that no external heat source is present in the system, we obtain the following heat balance equation:

$$\int_\Omega \rho[e(x,t) - e(x,0)]\,\mathrm{d}V = \int_0^t \int_{\partial\Omega} q(x,\tau)\mathrm{d}S\,\mathrm{d}\tau. \tag{7}$$

By definition (1), we have $e(x,0) = 0$. The bar has a constant cross-sectional area A and is thermally insulated at the end $x = l$ ($q(l,t) = 0$), as well as along its lateral surface. Consequently, heat exchange occurs only through the boundary at $x = 0$. Under these assumptions, Equation (7) can be rewritten as

$$A \int_0^l \rho e(x,t)\,\mathrm{d}x = A \int_0^t q(x,\tau)\mathrm{d}\tau. \tag{8}$$

We now observe that $e(x,t) = 0$ for $x > s(t)$, as stated in (1), and the heat is only stored in the liquid region. This allows us to express Equation (8) in the following form:

$$\int_0^{s(t)} \rho e(x,t)\,\mathrm{d}x = \int_0^t q(x,\tau)\mathrm{d}\tau. \tag{9}$$

Then, for an arbitrary point $x_1 \in (0,l)$, the balance can be expressed as

$$\int_{x_1}^{s(t)} \rho e(x,t)\,\mathrm{d}x = \int_0^t q(x_1,\tau)\mathrm{d}\tau. \tag{10}$$

However, since the point x_1 initially lies in the solid phase, the heat flux $q(x_1,\tau)$ vanishes for all $\tau < h(x_1)$, where $h(x_1) := s^{-1}(x_1)$ is the inverse of the free boundary $s(t)$, assumed to be increasing by hypothesis. At time $\tau = h(x_1)$, the phase change occurs and the point x_1 enters the liquid region and the flux becomes non-zero. Consequently, the balance simplifies to

$$\int_{x_1}^{s(t)} \rho e(x,t)\,\mathrm{d}x = \int_{h(x_1)}^t q(x_1,\tau)\mathrm{d}\tau. \tag{11}$$

We now apply the time derivative operator $\frac{\partial}{\partial t}$ to both sides of Equation (11)

$$\frac{\partial}{\partial t}\left(\int_{x_1}^{s(t)} \rho e(x,t)\,\mathrm{d}x\right) = \frac{\partial}{\partial t}\left(\int_{h(x_1)}^t q(x_1,\tau)\mathrm{d}\tau\right) = q(x_1,t). \tag{12}$$

Differentiating the left-hand side and replacing e by its definition in (1), we obtain

$$s'(t)\rho[\ell + c(u(s(t)^-,t) - U_m)] + \int_{x_1}^{s(t)} \frac{\partial}{\partial t}(\rho[\ell + c(u(x,t) - U_m)])\,\mathrm{d}x = q(x_1,t).$$

Taking into account our assumption that the temperature at the free boundary $s(t)$ corresponds to the phase-change temperature, that is, $u(s(t)^-,t) = U_m$, it follows that

$$s'(t)\rho\ell + \int_{x_1}^{s(t)} \rho c \frac{\partial}{\partial t} u(x,t)\,\mathrm{d}x = q(x_1,t). \tag{13}$$

And by the Fundamental Theorem of Calculus, we are allowed to write

$$q(s(t)^-,t) - q(x_1,t) = \int_{x_1}^{s(t)} \frac{\partial}{\partial x} q(x,t)\mathrm{d}t. \tag{14}$$

Now, if we substitute Equation (14) into Equation (13), and write the expression for the non-Fourier heat flux given in (2), we obtain

$$\int_{x_1}^{s(t)} \rho c \frac{\partial}{\partial t} u(x,t) - k_\alpha\, {}_0^C D_x^\alpha u(x,t)\mathrm{d}x + k_\alpha\, {}_0^C D_x^\alpha u_L(s(t)^-,t) + s'(t)\rho\ell = 0. \tag{15}$$

The same argument holds for any other point $x_2 > x_1$, leading to an analogous balance

$$\int_{x_2}^{s(t)} \rho c \frac{\partial}{\partial t} u(x,t) - k_\alpha\, {}_0^C D_x^\alpha u(x,t)\mathrm{d}x + k_\alpha\, {}_0^C D_x^\alpha u_L(s(t)^-,t) + s'(t)\rho\ell = 0. \tag{16}$$

Subtracting the energy balance at x_2 from that at x_1, we obtain

$$\int_{x_1}^{x_2} \rho c \frac{\partial}{\partial t} u(x,t) - k_\alpha\, {}_0^C D_x^\alpha u(x,t)\mathrm{d}x = 0$$

and using the fact that the interval (x_1, x_2) is arbitrary, it follows that

$$\rho c \frac{\partial}{\partial t} u(x,t) - k_\alpha \, {}_0^C D_x^\alpha u(x,t) = 0. \tag{17}$$

This yields an appropriate governing heat equation for the liquid phase. Furthermore, upon substituting (17) into (15) or (16), we can deduce the fractional Stefan condition

$$\rho \ell s'(t) = -k_\alpha \, {}_0^C D_x^\alpha u(s(t)^-, t). \tag{18}$$

The fractional Stefan condition expresses the balance of energy at the moving interface: the advance of the free boundary, $s'(t)$, is proportional to the heat flux that arrives at the interface from the liquid region. The presence of the fractional Caputo derivative in space, ${}_0^C D_x^\alpha u$, reflects the spatial nonlocal nature of the diffusion process. Unlike the classical derivative, the fractional operator captures and weighs the contributions of temperature variations throughout the domain $(0, s(t))$, rather than relying solely on local gradients. This leads to a more accurate description of anomalous diffusion phenomena, where the phase change dynamics depends on a broader range of spatial interactions within the material.

2.2. The Convective-Type Condition

The boundary of the domain is assumed to interact thermally with the external environment. This interaction can be modeled by convective-type boundary conditions, which represent the balance between conduction within the medium and convective heat exchange with the environment. These conditions are among the most prevalent in physical applications, particularly when the surface is exposed to a fluid or ambient medium at a prescribed temperature.

In this work, we propose a fractional extension of the classical convective boundary condition. This formulation is intended for use in models governed by fractional diffusion equations, where nonlocal effects may be relevant.

A convective-type boundary condition that incorporates Newton's law of cooling is now introduced. According to Newton's law of cooling, the heat flux at the boundary is expressed as

$$q = h\,(u(0,t) - U_\infty),$$

where h is the heat transfer coefficient, $u(0,t)$ is the boundary temperature, and U_∞ is the ambient temperature. In our fractional model, we generalize this classical flux by introducing the non-Fourier fractional flux $q(x,t)$ defined in (3).

The convective-type boundary condition then incorporates a rescaled time factor $t^{\frac{\alpha}{1+\alpha}}$, as a generalization of the classical model presented in [17], and is expressed at the boundary $x = 0$ as

$$k_\alpha \lim_{x \to 0^+} {}_0^C D_x^\alpha u(x,t) = \frac{h_\alpha}{t^{\frac{\alpha}{1+\alpha}}} (u(0,t) - U_\infty).$$

To maintain dimensional consistency with this time rescaling, we define $h_\alpha = \mu_\alpha h$, where μ_α is a constant introduced with dimensions $[\mu_\alpha] = [T^{\frac{\alpha}{1+\alpha}}]$, and $[T]$ is a unit of time. We suppose that $U_\infty > U_m$ (U_m the melting temperature).

Adding boundary and initial conditions, the one-phase fractional Stefan problem modeled by the non-Fourier flux is given by finding the temperature $u(x,t)$ and the free boundary $s(t)$ such that

$$\begin{array}{lll} \text{(i)} & \frac{\partial}{\partial t}u(x,t) = d_\alpha \frac{\partial}{\partial x}\, {}_0^C D_x^\alpha u(x,t), & 0 < x < s(t),\ 0 < t < T, \\ \text{(ii)} & k_\alpha \lim\limits_{x\to 0^+} {}_0^C D_x^\alpha u(x,t) = \frac{h_\alpha}{t^{\frac{\alpha}{1+\alpha}}}(u(0,t) - U_\infty), & 0 < t < T, \\ \text{(iii)} & u(s(t),t) = U_m, & 0 < t < T, \\ \text{(iv)} & s(0) = 0, & \\ \text{(v)} & \rho \ell s'(t) = -k_\alpha\, {}_0^C D_x^\alpha u(s(t)^-,t), & 0 < t < T. \end{array} \tag{19}$$

Here, we define $d_\alpha = \nu_\alpha d$, with $d = \frac{k}{\rho c}$ being the classical thermal diffusivity coefficient.

3. A Self-Similar Solution

The aim of this section is to obtain an exact solution to problem (19). We begin by seeking a self-similar solution using the method of self-similar variables presented in [15]. Then, consider a solution of the form

$$\Phi(z) := u(x,t), \text{where } z \text{ is the self-similar variable } z := \frac{x}{(d_\alpha t)^{\frac{1}{1+\alpha}}}. \tag{20}$$

Proceeding as in [15] (Section 4), we obtain the equivalent ordinary fractional equation associated with (19)-(i). More specifically,

$$0 = \frac{\partial}{\partial t}u(x,t) - d_\alpha \frac{\partial}{\partial x}\, {}_0^C D_x^\alpha u(x,t) = -\frac{1}{t}\left[\frac{z}{1+\alpha}\Phi'(z) + \frac{\partial}{\partial z}\, {}_0^C D_z^\alpha \Phi(z)\right]. \tag{21}$$

Then, letting $\sigma(z) = \Phi'(z)$, and using [18] (Theorem 2.1), which ensures that for all $f \in AC[a,b]$ satisfying ${}_aI^{1-\alpha}\frac{d}{dz}f \in AC[a,b]$ with $\alpha \in (0,1)$, it follows that

$$\frac{d}{dx}\, {}_a^C D_x^\alpha f(z) = {}_a^{RL} D_x^\alpha \left(\frac{d}{dz} f(z)\right) \quad \text{a.e. in } (a,b),$$

we obtain the desired fractional ODE

$$\frac{z}{1+\alpha}\sigma(z) + {}_0^{RL} D_z^\alpha \sigma(z) = 0. \tag{22}$$

In order to present the solution to Equation (22), we recall the following special function.

Definition 3. *Let $\alpha > 0$, $m > 0$, and l be such that $\alpha(jm+l) \neq -1, -2, -3, \ldots$ for all $j = 0, 1, 2, \ldots$. We define the three-parameter Mittag–Leffler function $E_{\alpha,m,l}(z)$ as*

$$E_{\alpha,m,l}(z) = \sum_{n=0}^{\infty} c_n z^n, \quad \text{with } c_0 = 1, \quad c_n = \prod_{j=0}^{n-1} \frac{\Gamma(\alpha(jm+l)+1)}{\Gamma(\alpha(jm+l+1)+1)}, \quad n \in \mathbb{N}. \tag{23}$$

By applying [19] (Theorem 4), a solution to (22) can be written as

$$\sigma(z) = z^{\alpha-1} E_{\alpha,1+\frac{1}{\alpha},1}\left(-\frac{z^{1+\alpha}}{1+\alpha}\right) = \sum_{n=0}^{\infty} c_n (-1)^n \frac{z^{(n+1)(1+\alpha)-2}}{(1+\alpha)^n}, \tag{24}$$

with c_n given by

$$c_0 = 1, \quad c_n = \prod_{j=0}^{n-1} \frac{\Gamma(j(\alpha+1)+\alpha+1)}{\Gamma(j(\alpha+1)+2\alpha+1)}, \quad n \in \mathbb{N}.$$

Therefore,

$$\Phi(z) = A + B\int_0^z w^{\alpha-1} E_{\alpha,1+\frac{1}{\alpha},1}\left(-\frac{w^{1+\alpha}}{1+\alpha}\right) \mathrm{d}w$$

is a solution to the fractional ODE in (21) for arbitrary constants A and B. Finally, we state that for each $A, B \in \mathbb{R}$, the function $u : \mathbb{R}_0^+ \times (0,T) \to \mathbb{R}$ defined by

$$u(x,t) = A + B\int_0^{x/(d_\alpha t)^{\frac{1}{1+\alpha}}} \sigma(w)\, \mathrm{d}w \tag{25}$$

is a solution to Equation (19)-(i).

In order to present some properties for the self-similar solution (25), we will show that its kernel, namely σ, is non-negative on $\mathbb{R}^+$. This result has been proven in [15]; however by following the ideas in [20] (Lemma A), an alternative simpler proof is presented here. Let us start with a previous result.

Proposition 1. *Let $\alpha \in (0,1)$ and $f \in AC[a,b]$. Then, the following relations hold for almost every $x \in (a,b)$:*

$${}_a^C D_x^\alpha f(x) = \frac{1}{\Gamma(1-\alpha)} \frac{f(x)-f(a)}{(x-a)^\alpha} + \frac{\alpha}{\Gamma(1-\alpha)} \int_0^x \frac{f(p)-f(x)}{(x-p)^{\alpha+1}}\, \mathrm{d}p, \tag{26}$$

and

$${}_a^{RL} D_x^\alpha f(x) = \frac{f(x)}{\Gamma(1-\alpha)(x-a)^\alpha} + \frac{\alpha}{\Gamma(1-\alpha)} \int_0^x \frac{f(p)-f(x)}{(x-p)^{\alpha+1}}\, \mathrm{d}p. \tag{27}$$

Proof. By hypothesis, we have that

$${}_a^C D_x^\alpha f(x) = \frac{1}{\Gamma(1-\alpha)} \int_0^x \frac{\frac{d}{dp}(f(p)-f(x))}{(x-p)^\alpha} \mathrm{d}p.$$

For fixed $x \in (a,b)$ and any $\epsilon > 0$, note that $\frac{1}{(x-p)^\alpha} \in AC[a, x-\epsilon]$. Thus, integration by parts gives

$$\int_0^{x-\epsilon} \frac{\frac{d}{dp}(f(p)-f(x))}{(x-p)^\alpha}\, \mathrm{d}p = \frac{f(p)-f(x)}{(x-p)^\alpha}\Big|_a^{x-\epsilon} + \alpha \int_0^{x-\epsilon} \frac{f(p)-f(x)}{(x-p)^{\alpha+1}}\, \mathrm{d}p. \tag{28}$$

Let us analyze the boundary terms of the first summand in (28) as $\epsilon \to 0$. At $p = a$, we obtain

$$-\frac{f(a)-f(x)}{(x-a)^\alpha}. \tag{29}$$

At $p = x-\epsilon$, from $f \in AC([x-\epsilon, x])$ and since x is a Lebesgue point of f', we have

$$\frac{f(x)-f(x-\epsilon)}{\epsilon} - f'(x) = \frac{1}{\epsilon}\int_0^\epsilon [f'(x-s)-f'(x)]\, \mathrm{d}s \to 0.$$

In other words,

$$f(x)-f(x-\epsilon) = \epsilon[f'(x)+b(\epsilon)], \quad \text{where } \lim_{\epsilon\to 0} b(\epsilon) = 0. \tag{30}$$

Hence,

$$\frac{f(x-\epsilon)-f(x)}{\epsilon^{\alpha}} = -\epsilon^{1-\alpha}[f'(x)+b(\epsilon)] \to 0 \quad \text{as } \epsilon \to 0. \tag{31}$$

Now consider the second term in (28) and prove that it converges to

$$\int_0^x \frac{f(p)-f(x)}{(x-p)^{\alpha+1}}\,\mathrm{d}p. \tag{32}$$

We start by examining the remaining part of the integral over the interval $[x-\epsilon, x]$, performing the change of variables $s = x-p$ and applying identity (30)

$$\int_{x-\epsilon}^x \frac{f(p)-f(x)}{(x-p)^{\alpha+1}}\,\mathrm{d}p = -f'(x)\int_0^{\epsilon} s^{-\alpha}\,ds - \int_0^{\epsilon} b(s)s^{-\alpha}\,\mathrm{d}s. \tag{33}$$

Clearly for the first integral in (33),

$$-f'(x)\frac{\epsilon^{1-\alpha}}{1-\alpha} \to 0 \quad \text{as } \epsilon \to 0. \tag{34}$$

For the second one (33), note that $q(s) = s^{-\alpha} \in L^1(0,\epsilon)$ for all $\epsilon > 0$, and $b(s) \in L^{\infty}(0,\epsilon)$ for small ϵ since $\lim_{\epsilon\to 0} b(\epsilon) = 0$. Thus, by Hölder's inequality we get

$$\left|\int_0^{\epsilon} b(s)s^{-\alpha}\,\mathrm{d}s\right| \le \|b(s)\|_{L^{\infty}(0,\epsilon)}\|s^{-\alpha}\|_{L^1(0,\epsilon)} \le \overline{C}\epsilon^{1-\alpha} \to 0. \tag{35}$$

Combining (34) and (35) with (33), the integral over $[x-\epsilon, x]$ vanishes as $\epsilon \to 0$. Hence, the integral in (32) is absolutely convergent, and

$$\left|\int_0^x \frac{f(p)-f(x)}{(x-p)^{\alpha+1}}\,\mathrm{d}p - \int_0^{x-\epsilon} \frac{f(p)-f(x)}{(x-p)^{\alpha+1}}\,\mathrm{d}p\right| \to 0.$$

Taking the limit $\epsilon \to 0$ in (28), the following holds:

$${}_a^C D_x^{\alpha} f(x) = \frac{1}{\Gamma(1-\alpha)}\frac{f(x)-f(a)}{(x-a)^{\alpha}} + \frac{\alpha}{\Gamma(1-\alpha)}\int_0^x \frac{f(p)-f(x)}{(x-p)^{\alpha+1}}\,\mathrm{d}p.$$

This completes the proof of (26). To prove (27), we use the known relation [18] (Theorem 2.1)

$${}_a^{RL} D_x^{\alpha} f(x) = {}_a^C D_x^{\alpha} f(x) + \frac{f(a)}{\Gamma(1-\alpha)}(x-a)^{-\alpha}. \tag{36}$$

Then, applying identity (26) to (36), we obtain

$${}_a^{RL} D_x^{\alpha} f(x) = \frac{f(x)}{\Gamma(1-\alpha)(x-a)^{\alpha}} + \frac{\alpha}{\Gamma(1-\alpha)}\int_0^x \frac{f(p)-f(x)}{(x-p)^{\alpha+1}}\,\mathrm{d}p.$$

□

Proposition 2. *Let $\alpha \in (0,1)$. Then the function $\sigma(x) = x^{\alpha-1}E_{\alpha,1+\frac{1}{\alpha},1}\left(-\frac{x^{1+\alpha}}{1+\alpha}\right)$ is non-negative on $\mathbb{R}^+$.*

Proof. Suppose this is not the case; that is, there exists at least one $x_1 > 0$ such that $\sigma(x_1) < 0$. Observe that

$$\sigma(0^+) = \lim_{x\to 0^+} x^{\alpha-1}E_{\alpha,1+\frac{1}{\alpha},1}\left(-\frac{x^{1+\alpha}}{1+\alpha}\right) = +\infty,$$

and that $\sigma \in C^1(\mathbb{R}^+)$. Therefore, the set

$$G := \{x > 0 : \sigma(x) < 0\}$$

is non-empty. Due to the continuity of $\sigma(x)$, there exists some $x_0 > 0$ such that

$$\sigma(x_0) = 0 \quad \text{and} \quad \sigma(x) > 0 \quad \forall x \in (0, x_0).$$

We can then apply Proposition 1, taking into account that $\sigma \in AC[a, b]$ for $0 < a < x_0$; i.e.,

$${}^{RL}_{a}D^{\alpha}_{x}\sigma(x) = \frac{\sigma(x)}{\Gamma(1-\alpha)(x-a)^{\alpha}} + \frac{\alpha}{\Gamma(1-\alpha)} \int_0^x \frac{\sigma(p) - \sigma(x)}{(x-p)^{\alpha+1}} \, \mathrm{d}p.$$

Letting $a \to 0$ on both sides, we obtain

$${}^{RL}_{0}D^{\alpha}_{x}\sigma(x) = \frac{\sigma(x)}{\Gamma(1-\alpha)x^{\alpha}} + \frac{\alpha}{\Gamma(1-\alpha)} \int_0^x \frac{\sigma(p) - \sigma(x)}{(x-p)^{\alpha+1}} \, \mathrm{d}p. \tag{37}$$

Since σ is a solution to Equation (22), it follows that ${}^{RL}_{0}D^{\alpha}\sigma(x_0) = 0$. However, evaluating (37) at x_0, we obtain

$${}^{RL}_{0}D^{\alpha}_{x}\sigma(x_0) = \frac{\alpha}{\Gamma(1-\alpha)} \int_0^{x_0} \frac{\sigma(p)}{(x_0-p)^{\alpha+1}} \, \mathrm{d}p > 0.$$

This contradiction comes from assuming that $\sigma(x) < 0$ for some $x \in (0, +\infty)$.

□

We now proceed to prove the main result.

Theorem 1. *Given $\alpha \in (0,1)$, $U_\infty, U_m \in \mathbb{R}$, and $h_\alpha, k_\alpha > 0$, Problem (19) admits a unique self-similar solution, which is given by*

$$u(x,t) = A + B \int_0^{x/(d_\alpha t)^{\frac{1}{1+\alpha}}} \sigma(p) \, \mathrm{d}p, \quad s(t) = \delta_\alpha (d_\alpha t)^{\frac{1}{1+\alpha}} \tag{38}$$

with

$$A = U_\infty + B\frac{\Gamma(\alpha)k_\alpha}{h_\alpha d_\alpha^{\frac{\alpha}{1+\alpha}}}, \quad B = -\frac{U_\infty - U_m}{\displaystyle\int_0^{\delta_\alpha} \sigma(p) \, \mathrm{d}p + \frac{\Gamma(\alpha)k_\alpha}{h_\alpha d_\alpha^{\frac{\alpha}{1+\alpha}}}}$$

and $\delta_\alpha > 0$, which is the unique solution to the equation $H_\alpha(x) = x$, where $H_\alpha : \mathbb{R}_0^+ \to \mathbb{R}$ is defined by

$$H_\alpha(x) = \frac{k_\alpha(U_\infty - U_m)}{\rho \ell d_\alpha} \frac{(1+\alpha)\Gamma(\alpha) - \displaystyle\int_0^x p\sigma(p) \, \mathrm{d}p}{\displaystyle\int_0^x \sigma(p) \, \mathrm{d}p + \frac{\Gamma(\alpha)k_\alpha}{h_\alpha d_\alpha^{\frac{\alpha}{1+\alpha}}}}. \tag{39}$$

Proof. Since $u(x,t)$ is of the form (25), it satisfies (19)-(i). We want to determine A and B so that u satisfies the remaining conditions.

From (19)-(iii) we see that

$$u(s(t),t) = A + B \int_0^{s(t)/(d_\alpha t)^{\frac{1}{1+\alpha}}} \sigma(p) \, \mathrm{d}p = U_m \quad \forall t \in (0,T),$$

and differentiating with respect to t yields

$$\frac{d}{dt}u(s(t),t) = \sigma\left(\frac{s(t)}{(d_\alpha t)^{\frac{1}{1+\alpha}}}\right)\frac{d}{dt}\left(\frac{s(t)}{(d_\alpha t)^{\frac{1}{1+\alpha}}}\right) = 0.$$

Then, by Proposition 2 we conclude that

$$s(t) = \delta_\alpha (d_\alpha t)^{\frac{1}{1+\alpha}}, \quad \text{for some } \delta_\alpha \in \mathbb{R}, \quad t \in (0,T). \tag{40}$$

We now examine condition (19)-(ii). Clearly $u(0,t) = A$. For the fractional flux we use the following identity established in [15] (Prop. 7):

$${}_0^C D_x^\alpha u(x,t) = B\Gamma(\alpha)(d_\alpha t)^{-\frac{\alpha}{1+\alpha}} - \frac{B(d_\alpha t)^{-\frac{\alpha}{1+\alpha}}}{1+\alpha}\int_0^{x/(d_\alpha t)^{\frac{1}{1+\alpha}}} p^\alpha E_{\alpha,1+\frac{1}{\alpha},1}\left(-\frac{p^{1+\alpha}}{1+\alpha}\right)\mathrm{d}p, \tag{41}$$

from where

$$\lim_{x\to 0^+} {}_0^C D_x^\alpha u(x,t) = \lim_{x\to 0^+} B\left(\frac{\Gamma(\alpha)}{(d_\alpha t)^{\frac{\alpha}{1+\alpha}}} - \sum_{n=1}^{\infty} c_{n-1}\frac{(-1)^{n-1}}{n(1+\alpha)^{n+1}}\frac{x^{n(1+\alpha)}}{(d_\alpha t)^{n+1-\frac{1}{1+\alpha}}}\right) = B\frac{\Gamma(\alpha)}{(d_\alpha t)^{\frac{\alpha}{1+\alpha}}}. \tag{42}$$

Hence, replacing (25) and (42) in (19)-(ii) it follows that

$$U_\infty + B\frac{\Gamma(\alpha)k_\alpha}{h_\alpha d_\alpha^{\frac{\alpha}{1+\alpha}}} = A. \tag{43}$$

Now, from (19)-(iii) we get

$$u(s(t),t) = A + B\int_0^{\delta_\alpha}\sigma(p)\mathrm{d}p = U_m. \tag{44}$$

Substituting the expression for A from (43) in (44) gives

$$U_\infty + B\frac{\Gamma(\alpha)k_\alpha}{h_\alpha d_\alpha^{\frac{\alpha}{1+\alpha}}} + B\int_0^{\delta_\alpha}\sigma(p)\mathrm{d}p = U_m. \tag{45}$$

Rewriting Equation (45) in terms of B, we obtain

$$B = -\frac{U_\infty - U_m}{\displaystyle\int_0^{\delta_\alpha}\sigma(p)\,\mathrm{d}p + \frac{\Gamma(\alpha)k_\alpha}{h_\alpha d_\alpha^{\frac{\alpha}{1+\alpha}}}}. \tag{46}$$

Note that the denominator is non-zero from Proposition 2, since $h_\alpha, k_\alpha > 0$.
To determine δ_α, consider condition (19)-(v)

$$\rho\ell s'(t) = -k_\alpha({}_0^C D_x^\alpha u)(s(t)^-,t), \quad 0 < t < T.$$

Substituting the expression (40) for $s(t)$, and applying the identity (41) into (19)-(v), we obtain

$$\delta_\alpha\frac{\rho\ell d_\alpha}{1+\alpha}(d_\alpha t)^{-\frac{\alpha}{1+\alpha}} = -k_\alpha\left(\Gamma(\alpha)B(d_\alpha t)^{-\frac{\alpha}{1+\alpha}} - \frac{B(d_\alpha t)^{-\frac{\alpha}{1+\alpha}}}{1+\alpha}\int_0^{\delta_\alpha} p\sigma(p)\,\mathrm{d}p\right). \tag{47}$$

Then for (46) and (47), we get

$$\delta_\alpha = \frac{k_\alpha(U_\infty - U_m)}{\rho \ell d_\alpha} \frac{(1+\alpha)\Gamma(\alpha) - \int_0^{\delta_\alpha} p\sigma(p)\mathrm{d}p}{\int_0^{\delta_\alpha} \sigma(p)\mathrm{d}p + \frac{\Gamma(\alpha)k_\alpha}{h_\alpha d_\alpha^{\frac{\alpha}{1+\alpha}}}}.$$

We are thus looking for a positive number δ_α satisfying $H_\alpha(x) = x$ for every $x > 0$, where the function H_α is given by (39).

Note that, by Proposition 2, we have

$$\lim_{x \searrow 0} \int_0^x p\sigma(p)\mathrm{d}p = 0^+ \quad \text{and} \quad \lim_{x \searrow 0} \int_0^x \sigma(p)\mathrm{d}p = 0^+.$$

Then

$$H_\alpha(0^+) = \frac{k_\alpha(U_\infty - U_m)}{\rho \ell d_\alpha} \frac{\Gamma(\alpha)(1+\alpha)}{\frac{\Gamma(\alpha)k_\alpha}{h_\alpha d_\alpha^{\frac{\alpha}{1+\alpha}}}} = (U_\infty - U_m)(1+\alpha)\frac{h_\alpha}{\rho \ell d_\alpha^{\frac{1}{1+\alpha}}} > 0. \tag{48}$$

Now from direct calculation we have

$$H'_\alpha(x) = -\frac{k_\alpha(U_\infty - U_m)}{\rho \ell d_\alpha} \frac{\sigma(x)\left[\Gamma(\alpha)(1+\alpha) + \frac{x\Gamma(\alpha)k_\alpha}{h_\alpha d_\alpha^{\frac{\alpha}{1+\alpha}}} + \int_0^x (x-p)\sigma(p)\mathrm{d}p\right]}{\left(\int_0^x \sigma(p)\mathrm{d}p + \frac{\Gamma(\alpha)k_\alpha}{h_\alpha d_\alpha^{\frac{\alpha}{1+\alpha}}}\right)^2}. \tag{49}$$

and since $\sigma(x) \geq 0$ for $x > 0$, we find

$$-\frac{k_\alpha(U_\infty - U_m)}{\rho \ell d_\alpha}\sigma(x)\left[\Gamma(\alpha)(1+\alpha) + \frac{x\Gamma(\alpha)}{h_\alpha d_\alpha^{\frac{\alpha}{1+\alpha}}} + \int_0^x (x-p)\sigma(p)\mathrm{d}p\right] < 0, \ \forall x > 0, \tag{50}$$

From (48) and (50), we conclude that

$$H_\alpha(0^+) = (U_\infty - U_m)(1+\alpha)\frac{h_\alpha}{\rho \ell d_\alpha^{\frac{1}{1+\alpha}}} > 0, \quad \text{and} \quad H'_\alpha(x) < 0 \,\forall\, x > 0,$$

which implies the existence of a unique $\delta_\alpha > 0$ such that $\delta_\alpha = H_\alpha(\delta_\alpha)$.

□

Remark 1. *It is worth noting that, to the best of our knowledge, a general proof of existence and/or regularity for the general space-fractional Stefan problem with Robin-type specification at the fixed boundary has not yet been addressed in the literature. There are recent results on existence, unicity, and regularity for the Neumann case, both for regular regions ($s(0) = b > 0$) and singular regions ($s(0) = 0$) in [21]. The Dirichlet case was addressed by the same authors by following the ideas in [22]. However, the Robin case remains an open problem regarding general existence, regularity, and uniqueness.*

Remark 2. *Note that an instantaneous phase change in a melting problem is guaranteed if we ask that $U_\infty > U_m$ and Newton's coefficient of heat transfer h is positive. In fact, we have assumed that*

the bar is at its melting temperature at the initial time and evaluating (38) *at the fixed face* $x = 0$ *yields*

$$u(0,t) = U_\infty - \frac{U_\infty - U_m}{\frac{h_\alpha d_\alpha^{\frac{\alpha}{1+\alpha}}}{\Gamma(\alpha)k_\alpha}\int_0^{\delta_\alpha}\sigma(p)\mathrm{d}p + 1} > U_m \iff (U_\infty - U_m)\left(\frac{h_\alpha d_\alpha^{\frac{\alpha}{1+\alpha}}}{\Gamma(\alpha)k_\alpha}\int_0^{\delta_\alpha}\sigma(p)\mathrm{d}p\right) > 0.$$

4. Numerical Solutions and Computational Experiments

4.1. Dimensionless Form

To implement numerical methods and improve the understanding of the essential behavior of the system, we reformulate problem (19) using dimensionless variables.

This process reduces the number of physical parameters in the problem, leading to two important dimensionless parameters that will take part in the new formulation. On the one side is the Stefan number (Ste), which expresses the ratio of sensible to latent heat. It governs the energy balance at the moving interface and determines the interface propagation rate. On the other side is the Biot number (Bi), which relates heat transfer by conduction within a body to heat transfer by convection at its surface.

To start our derivations of the dimensionless problem formulations, we identify the dimensions of the problem properties in Table 1.

To deal with fractional operators and dimensions, we use the following equalities stated in [23] (Proposition 1),

$$\left[{}_0^C D_x^\alpha f\right] = \frac{[f]}{[L^\alpha]}, \quad \left[\frac{\partial}{\partial x}\,{}_0^C D_x^\alpha f\right] = \frac{[f]}{[L^{1+\alpha}]}, \quad \left[{}_0^{RL} D_x^\alpha f\right] = \frac{[f]}{[L^\alpha]}, \text{for every } \alpha \in (0,1).$$

To derive a dimensionless version of the original model, we perform the following change of variables:

$$y = \frac{x}{x_0}, \quad \tau = \frac{t}{t_0}, \quad t_0 = \frac{x_0^2}{d} \tag{51}$$

where x_0 and t_0 are the characteristic position and time and introduce the dimensionless temperature

$$w(y,\tau) = \frac{u(x(y),t(\tau)) - U_m}{\Delta U}, \text{ for } \Delta U = U_\infty - U_m. \tag{52}$$

Finally, consider the admissible parameters

$$\nu_\alpha = x_0^{\alpha-1}, \quad \mu_\alpha = t_0^{\frac{\alpha}{1+\alpha}}. \tag{53}$$

Note that there is no natural characteristic length x_0 for this problem. However, this does not pose any difficulties for the modeling, as we will see in Section 4.3.4.

With the previous definitions, the temporal and spatial derivatives transform as

$$w_\tau(y,\tau) = \frac{t_0}{\Delta U}\,u_t(x,t), \quad w_y(y,\tau) = \frac{x_0}{\Delta U}\,u_x(x,t) \tag{54}$$

and the Caputo fractional derivative and its derivative as

$${}_0^C D_y^\alpha w(y,\tau) = \frac{x_0^\alpha}{\Delta U}\,{}_0^C D_x^\alpha u(x,t) \quad \text{and} \quad \frac{\partial}{\partial y}\,{}_0^C D_y^\alpha w(y,\tau) = \frac{x_0^{1+\alpha}}{\Delta U}\frac{\partial}{\partial x}\,{}_0^C D_x^\alpha u(x,t). \tag{55}$$

From (53), (54), and (55), the original FDE (19)-(i) leads to the following dimensionless form:

$$w_\tau(y,\tau) = \frac{\partial}{\partial y}\, {}_0^C D_y^\alpha w(y,\tau). \tag{56}$$

To ensure dimensional consistency, we verify

$$[\nu_\alpha][x_0]^{1-\alpha}\left[\frac{\partial}{\partial y}\, {}_0^C D_y^\alpha w\right] = [L^{\alpha-1}][L^{1-\alpha}][-] = [-]. \tag{57}$$

From (19)-(ii), (52), and (55), we have the rescaled boundary condition

$$\lim_{y\to 0^+} {}_0^C D_y^\alpha w(y,\tau) = \frac{x_0 h}{k}\frac{1}{\tau^{\frac{\alpha}{1+\alpha}}}(w(0,\tau)-1),$$

where

$$[\frac{x_0 h}{k}] = [x_0][\frac{1}{k}][h] = [L][\frac{\Theta T^3}{ML}][\frac{M}{T^3\Theta}] = [-].$$

For the rescaled interface we have

$$\xi(\tau) = \frac{s(t(\tau))}{x_0}, \quad \xi'(\tau) = \frac{t_0}{x_0}s'(t(\tau)), \tag{58}$$

Then, from (19)-(v), (55), and (58) we obtain the transformed fractional Stefan condition

$$\xi'(\tau) = -\frac{c\Delta U}{\ell}\, {}_0^C D_y^\alpha w(\xi(\tau)^-,\tau).$$

Adding appropriate initial conditions for the rescaled temperature w and the rescaled moving interface ξ and defining the dimensionless Stefan and Biot numbers by $r\text{Ste} = \frac{c\Delta U}{\ell}$ and $\text{Bi} = \frac{x_0 h}{k}$, respectively and defining $\tau_T = \frac{T}{T_0}$, we complete the nondimensional formulation of the system as follows:

$$\begin{array}{lll}
\text{(i)} & w_\tau(y,\tau) = \frac{\partial}{\partial y}\, {}_0^C D_y^\alpha w(y,\tau), & 0<y<\xi(t),\ 0<\tau<\tau_T,\\
\text{(ii)} & \lim\limits_{y\to 0^+} {}_0^C D_y^\alpha w(y,\tau) = \frac{\text{Bi}}{\tau^{\frac{\alpha}{1+\alpha}}}(w(0,\tau)-1), & 0<\tau<\tau_T,\\
\text{(iii)} & w(\xi(\tau),\tau) = 0, & 0<\tau<\tau_T,\\
\text{(iv)} & \xi(0) = 0, & \\
\text{(v)} & \xi'(\tau) = -\text{Ste}\, {}_0^C D_y^\alpha w(\xi(\tau)^-,\tau), & 0<\tau<\tau_T.
\end{array} \tag{59}$$

This dimensionless formulation provides a more compact and insightful representation of the problem, establishing a solid foundation for both analytical methods and numerical simulations.

4.2. Numerical Method

We describe now the algorithm implemented to obtain and plot the free boundary corresponding to the solution of (59). For the reader's convenience, we recall here the equations used in the numerical implementation, including the expressions for σ, w, and ξ, as well as the characteristic condition for δ_α involving the function H_α, as implemented in the Python code. Here σ is the function defined in (24) for $B = 1$ and $d_\alpha = 1$. The general solution is given by

$$\xi(\tau) = \delta_\alpha \tau^{\frac{1}{1+\alpha}}, \quad w(y,\tau) = A + B\int_0^{y/\tau^{\frac{1}{1+\alpha}}} \sigma(p)\, \mathrm{d}p \tag{60}$$

with

$$A = 1 - \frac{\Gamma(\alpha)}{\mathrm{Bi}\displaystyle\int_0^{\delta_\alpha} \sigma(p)\mathrm{d}p + \Gamma(\alpha)}, \quad B = -\frac{1}{\displaystyle\int_0^{\delta_\alpha} \sigma(p)\mathrm{d}p + \frac{\Gamma(\alpha)}{\mathrm{Bi}}} \tag{61}$$

and $\delta_\alpha > 0$, which is the unique solution to the equation $H_\alpha(y) = y$, where $H_\alpha : \mathbb{R}_0^+ \to \mathbb{R}$ is defined by

$$H_\alpha(y) = \mathrm{Ste}\frac{(1+\alpha)\Gamma(\alpha) - \displaystyle\int_0^y p\sigma(p)\mathrm{d}p}{\displaystyle\int_0^y \sigma(p)\mathrm{d}p + \frac{\Gamma(\alpha)}{\mathrm{Bi}}}. \tag{62}$$

Note that the function w in (60) can be expressed as series by

$$w(y,\tau) = A + B\sum_{n=0}^{\infty} \frac{c_n(-1)^n}{(1+\alpha)^n} \frac{y^{(n+1)(1+\alpha)-1}}{[(n+1)(1+\alpha)-1]\tau^{\frac{(n+1)(1+\alpha)-1}{1+\alpha}}}, \tag{63}$$

which is an absolutely convergent series on compact subsets of $\mathbb{R}_0^+ \times (0,T)$.

For the numerical implementation, we relied on the value of δ_α, determined as the solution of the nonlinear equation $y = H_\alpha(y)$ arising from the self-similar formulation of the problem. To this end, we employed a bisection method.

The code also includes functions to approximate the integrals

$$\int_0^y p\,\sigma(p)\mathrm{d}p \quad \text{and} \quad \int_0^y \sigma(p)\mathrm{d}p,$$

which are required in the evaluation of the function $H_\alpha(y)$ during the iterative process. To ensure accurate and efficient computations, we take advantage of the series representation of the Mittag–Leffler function. In this way, both integrals can be expanded into convergent series, leading to explicit expressions

$$\int_0^x \sigma_\alpha(p)\mathrm{d}p = \sum_{n=0}^{\infty} \frac{c_n(-1)^n}{(1+\alpha)^n} \frac{x^{(n+1)(1+\alpha)-1}}{(n+1)(1+\alpha)-1}, \tag{64}$$

and

$$\int_0^x p\sigma_\alpha(p)\mathrm{d}p = \sum_{n=0}^{\infty} \frac{c_n(-1)^n}{(1+\alpha)^n} \frac{x^{(n+1)(1+\alpha)}}{(n+1)(1+\alpha)}. \tag{65}$$

Here, $\{c_n\}_{n\geq 0}$ denotes the sequence defined by (23) for $m = 1 + \frac{1}{\alpha}, l = 1$:

$$c_0 = 1, \qquad c_n = \prod_{j=0}^{n-1} \frac{\Gamma\big(j(\alpha+1)+\alpha+1\big)}{\Gamma\big(j(\alpha+1)+2\alpha+1\big)}, \quad n \in \mathbb{N}.$$

Since the series are alternating, the truncation error after M terms can be bounded by estimating the magnitude of the $(M+1)$-th terms in expansions (64) and (65), namely

$$a_{M+1} := \frac{c_{M+1}}{(1+\alpha)^{M+1}} \frac{x^{(M+2)(1+\alpha)-1}}{(M+2)(1+\alpha)-1}, \qquad b_{M+1} := \frac{c_{M+1}}{(1+\alpha)^{M+1}} \frac{x^{(M+2)(1+\alpha)}}{(M+2)(1+\alpha)}.$$

Furthermore, by employing the recursive relation

$$c_n = c_{n-1} \frac{\Gamma\big(n(1+\alpha)\big)}{\Gamma\big(n(1+\alpha)+\alpha\big)},$$

together with Gautschi's inequality [24] to estimate the quotient of Gamma functions, we obtain

$$c_n < \frac{c_{n-1}}{(n(1+\alpha)+\alpha-1)^\alpha} < \frac{c_{n-1}}{(n-1)^\alpha(1+\alpha)^\alpha} < \frac{c_{n-1}}{(n-1)^\alpha} < \frac{1}{(n-1)!^\alpha}.$$

Consequently, both error terms for $x \in [0, l]$ satisfy the bounds

$$a_{M+1},\, b_{M+1} \;<\; \frac{1}{M!^\alpha}\frac{x^{(M+2)(1+\alpha)}}{(M+1)^\alpha} < \frac{l^{2(M+2)}}{(M+1)!^\alpha}.$$

The root-finding step is performed using the bisection method, with the error after k iterations bounded by $l/2^k$, where l is the length of the initial interval. As an illustrative example, taking $l = 2$ and $M = 30$, both series (64) and (65) are approximated with an error smaller than

$$a_{31},\, b_{31} \;<\; 3.59 \times 10^{-14}.$$

Furthermore, if the bisection method is applied to calculate the root, after $k = 50$ iterations, the error in the calculated root is bounded by $1/2^{49} < 10^{-14}$, showing that the overall numerical procedure achieves a very high accuracy.

All simulations and numerical computations were performed using Python 3.11 on a computer system equipped with an AMD Ryzen 5 5500U processor (6 cores, 12 threads, 2.10 GHz base clock) and 8 GiB of DDR4 RAM and running a Windows-based operating system. For a more in-depth analysis and to access the implementation details, the reader is referred to [16].

4.3. Model Analysis via Numerical Experiments

In this section, we present numerical simulations of the model, focusing on the shape of the interface. In order to explore the behavior of the solution under different physical regimes, we conduct three numerical experiments. The first one focuses on the fractional order α and its relation to the classical Stefan problem with convective boundary condition when the classical derivative is recovered by taking $\alpha = 1$. For the second and the third experiments, we vary the Stefan and the Biot numbers along with the order of differentiation α.

4.3.1. Variation in the Fractional Order α

We begin by performing an analytical examination of the model (59) in the classical case $\alpha = 1$, which corresponds to the standard Stefan problem with a convective boundary condition. To facilitate comparison and isolate the effect of the fractional order, we fix the Stefan and Biot numbers to $\mathrm{Ste} = \mathrm{Bi} = 1$. For $\alpha = 1$ in (59), we have

$$\begin{array}{lll}
\text{(i)} & w_\tau(y,\tau) = w_{yy}(y,\tau), & 0 < y < \xi(t),\ 0 < \tau < \tau_T, \\
\text{(ii)} & \lim\limits_{y\to 0^+} w_y(y,\tau) = \frac{1}{\tau^{1/2}}(w(0,\tau)-1), & 0 < \tau < \tau_T, \\
\text{(iii)} & w(\xi(\tau),\tau) = 0, & 0 < \tau < \tau_T, \\
\text{(iv)} & \xi(0) = 0, & \\
\text{(v)} & \xi'(\tau) = -\, w_y(\xi(\tau)^-,\tau), & 0 < \tau < \tau_T.
\end{array} \tag{66}$$

The solution to Problem (66) was obtained in [17] (Theorem 2) and is given by

$$w_1(y,\tau) = A + B\sqrt{\pi}\,\mathrm{erf}\left(\frac{y}{2\sqrt{\tau}}\right), \tag{67}$$

$$s_1(\tau) = \delta_1 \tau^{1/2}, \quad \tau \in (0, T),$$

where $B = -\frac{1}{1+\sqrt{\pi}\text{erf}(\text{ffi}_1/2)}$, $A = 1 + B$, and δ_1 is the unique solution of the equation

$$H_1(y) = y, \quad y > 0,$$

with

$$H_1(y) = \frac{2e^{-\left(\frac{y}{2}\right)^2}}{\sqrt{\pi}\,\text{erf}\left(\frac{y}{2}\right) + 1}.$$

Now that we have an explicit expression for the classical solution, we compare this case with our numerical simulation for the fractional model for $\alpha = 1$. As shown in Figure 1, this comparison demonstrates that the series solution provides an accurate estimate of the classical case, since it produces the same value of δ_1, namely $\delta_1 = 0.892402$, up to seven significant digits.

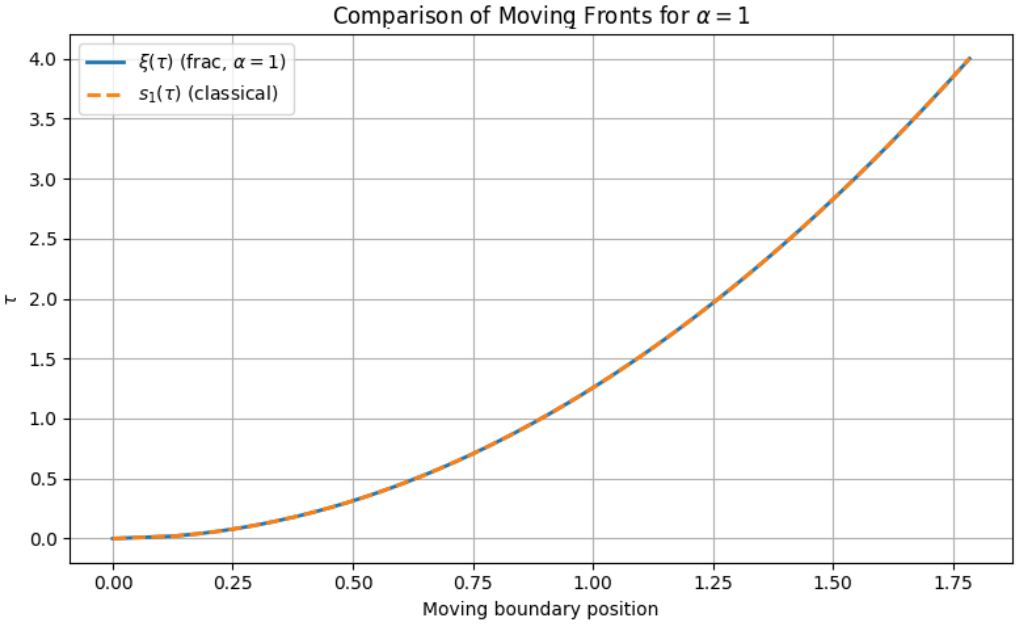

Figure 1. Comparison between the analytical classical solution and the fractional numerical series solution for $\alpha = 1$.

Let us now analyze how changes in the fractional order α affect the behavior of the solution. We consider several values of α within the interval $(0, 1]$ with fixed $Ste = Bi = 1$ and observe their impact on the evolution of the free boundary. We focus on values of α approaching 1 to examine the transition toward the classical diffusion regime.

We observe in Figure 2 that for values of $\alpha < 1$, the free boundary exhibits a superdiffusive behavior: its progression is slower at early times and accelerates at later times. Also observing Table 2, we note that the values of δ_α increase monotonically as $\alpha \to 1$. Since the free boundary evolves proportionally to $t^{\frac{1}{1+\alpha}}$, the increase in the parameter δ_α partially counterbalances, at early times, the slower temporal growth imposed by the fractional exponent. As a result, the superdiffusive characteristic becomes more evident at larger times, where the effect of the power-law term dominates the dynamics and leads to a faster advancement of the front.

Table 2. Values of δ_α for different values of α.

α	0.5000	0.6000	0.7000	0.7500	0.8000	0.8500	0.9000	0.9500	1.0000
δ_α	0.700843	0.739294	0.777577	0.796692	0.815805	0.834926	0.854061	0.873218	0.892402

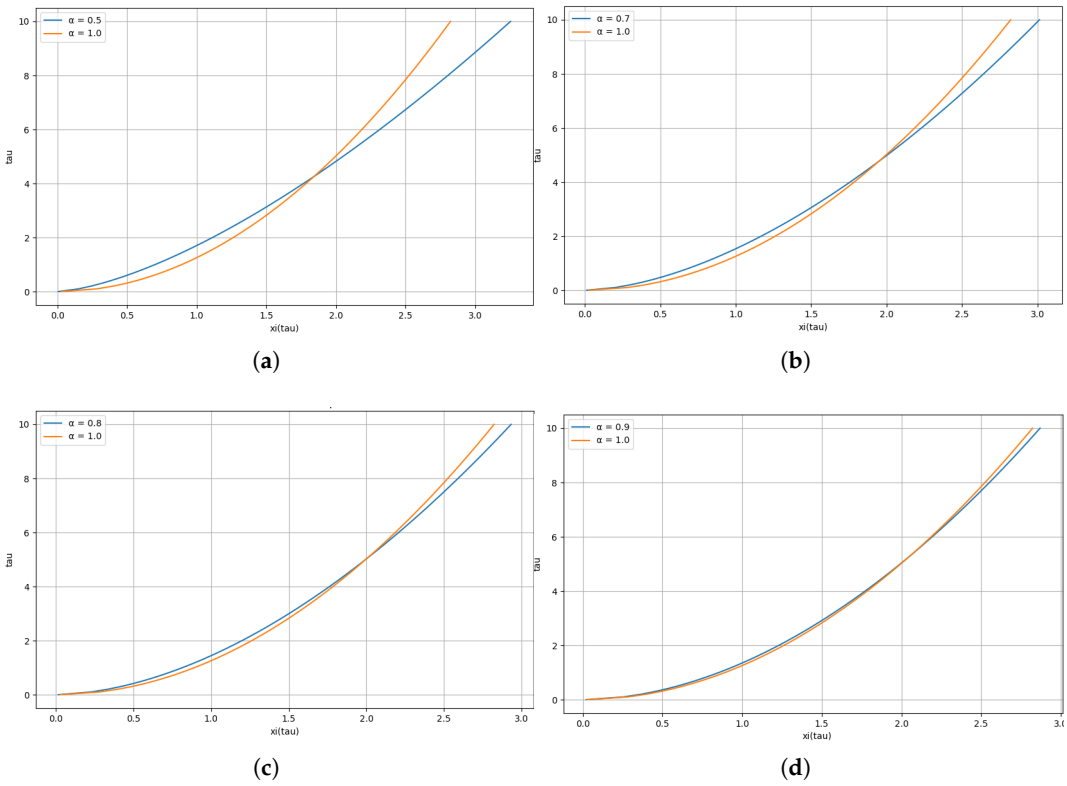

Figure 2. Comparison for multiple values of α. (**a**) $\alpha = 0.5$ vs. $\alpha = 1$; (**b**) $\alpha = 0.7$ vs. $\alpha = 1$; (**c**) $\alpha = 0.8$ vs. $\alpha = 1$; and (**d**) $\alpha = 0.9$ vs. $\alpha = 1$.

4.3.2. Variation in the Stefan Number *Ste*

The second experiment focuses on the influence of the Stefan number *Ste*, which characterizes the ratio between sensible and latent heat. By modifying *Ste*, we explore the shape of the free boundary. We consider values of *Ste* between zero and three with fixed $Bi = 1$ and analyze their effects on the interface, which can be seen in Figure 3 and Table 3.

It is worth noting that situations where the sensible heat is much smaller than the latent heat are common in nature. Although the Stefan number also depends on a reference temperature, it is standard in modeling classical materials to consider small values of this parameter (see, e.g., [25]). Therefore, it is reasonable to expect that the case of small Stefan numbers is also relevant for anomalous materials such as crystals or polymers.

Table 3. Values of δ_α for fixed Biot number Bi $= 1$ and varying Stefan numbers Ste.

$\alpha \setminus$ Ste	0.001	0.1	0.5	0.7	0.8	1	2	3
0.50	0.00144	0.10853	0.41407	0.53696	0.59394	0.70084	1.14361	1.49870
0.60	0.00156	0.12075	0.44770	0.57424	0.63208	0.73929	1.16738	1.49522
0.70	0.00168	0.13302	0.48163	0.61163	0.67023	0.77758	1.19109	1.49332
0.80	0.00179	0.14530	0.51585	0.64916	0.70845	0.81581	1.21525	1.49392
0.90	0.00189	0.15757	0.55035	0.68684	0.74676	0.85406	1.24024	1.49767
1.00	0.00200	0.16980	0.58512	0.72468	0.78519	0.89240	1.26628	1.50492

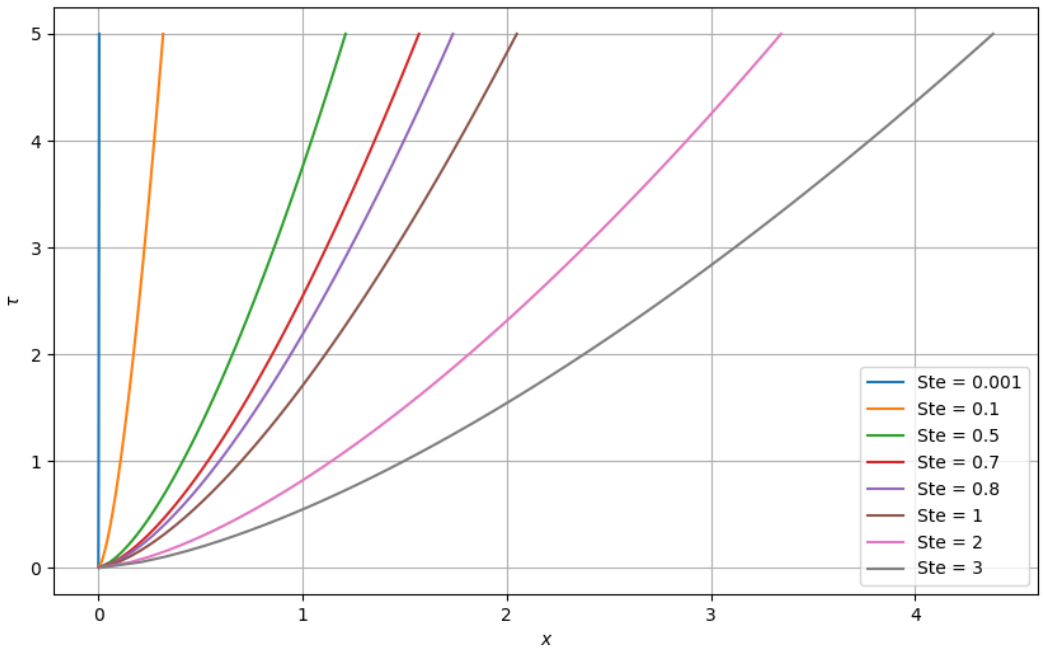

Figure 3. Effect of different Stefan numbers Ste on the time evolution of the free boundary for fixed $\alpha = 0.5$ and $Bi = 1$.

Let us now assume that the Stefan number is small, $Ste << 1$. In this regime, we also expect δ_α to be small. Approximating the integrals of the special functions in (62) by the first-order terms of their series representation and substituting them accordingly, it follows that, for small values of y, the equation reduces to the following power-series approximation.

$$Ste\,(1+\alpha)\Gamma(2+\alpha) = y^{1+\alpha}(\alpha\,Ste + 1 + \alpha) + y\frac{\Gamma(2+\alpha)}{Bi}. \tag{68}$$

It follows from a simple observation that columns 1 and 2 of Tables 3 and 4 coincide up to three significant digits. The previous observation confirms the accuracy of Equation (68) and serves as a validation of the numerical method presented in Section 4.2.

Table 4. Approximate values of δ_α for fixed Biot number Bi $= 1$ and varying Stefan numbers Ste using Equation (68).

$\alpha \setminus$ Ste	0.001	0.1	0.5	0.7
0.50	0.00144	0.10839	0.40752	0.52325
0.60	0.00156	0.12063	0.44117	0.56048
0.70	0.00168	0.13291	0.47527	0.59817
0.80	0.00179	0.14522	0.50978	0.63623
0.90	0.00189	0.15750	0.54464	0.67461
1.00	0.00200	0.16975	0.57980	0.71324

4.3.3. Variation in the Biot Number Bi

In the third experiment, we vary the Biot number Bi, which characterizes the ratio between convective heat transfer and thermal conductivity. For Bi $\to$ 0, Equation (59) implies that the fixed face is thermally insulated, resulting in a fully insulated bar that does not melt. Since this case is not of practical interest, it will not be considered further. Instead, we focus on large values of Bi to analyze the behavior of the interface and compare the limiting case with the solution to problem (59) under a Dirichlet boundary condition. We expect that these solutions coincide, according to the previous results in the literature for the classical case given in [17,26].

More explicitly, let us present the model when Bi approaches infinity. Using (61), we deduce that

$$A \to 1, \quad \text{and} \quad B \to -\frac{1}{\int_0^{\delta_\alpha} \sigma(p)\mathrm{d}p}, \qquad \text{as Bi} \to \infty. \tag{69}$$

The limit equation related to (62) is given by $G_\alpha(y) = y$, where $G_\alpha : \mathbb{R}_0^+ \to \mathbb{R}$ is defined by

$$G_\alpha(y) = \mathrm{Ste}\frac{(1+\alpha)\Gamma(\alpha) - \int_0^y p\sigma(p)\mathrm{d}p}{\int_0^y \sigma(p)\mathrm{d}p}.$$

Now, mimicking the proof of Theorem 1, it is straightforward to verify that the pair (w_∞, ξ_∞) given by

$$w_\infty(y,\tau) = 1 - \frac{\int_0^{y/\tau^{\frac{1}{1+\alpha}}} \sigma(p)\mathrm{d}p}{\int_0^{\delta_\infty} \sigma(p)\mathrm{d}p}, \quad \text{and} \quad \xi_\infty(\tau) = \delta_\infty \tau^{\frac{1}{1+\alpha}},$$

where δ_∞ is the unique solution to the equation $y = G_\alpha(y)$, is a solution to the following fractional Stefan problem with a constant Dirichlet condition:

$$\begin{array}{lll}
\text{(i)} & w_\tau(y,\tau) = \frac{\partial}{\partial y}\, {}_0^C D_y^\alpha w(y,\tau), & 0 < y < \xi(t),\ 0 < \tau < \tau_T, \\
\text{(ii)} & w(0,\tau) = 1, & \\
\text{(iii)} & w(\xi(\tau),\tau) = 0, & 0 < \tau < \tau_T, \\
\text{(iv)} & \xi(0) = 0, & \\
\text{(v)} & \xi'(\tau) = -\mathrm{Ste}\, {}_0^C D_y^\alpha w(\xi(\tau)^-,\tau), & 0 < \tau < \tau_T.
\end{array} \tag{70}$$

By comparing the coefficients of w_∞ with the limiting coefficients in (69), we are led to ask whether δ_α converges to δ_∞ when Bi $\to \infty$. Establishing this rigorously is a challenging mathematical problem that will be addressed in a separate theoretical paper. Our present aim is to numerically verify the aforementioned convergence.

The results are illustrated in Figure 4 for $\alpha = 0.5$ and $Ste = 1$ and in Table 5 for values of α between 0.5 and 1, with $Ste = 1$. In both cases, the expected convergence in the limiting case can be clearly observed.

Table 5. Values of δ_α for a fixed Stefan number Ste $= 1$ and varying Biot numbers Bi. The column corresponding to Bi $= \infty$ was obtained from a numerical method adapted to problem (70).

$\alpha \setminus$ Bi	1	3	5	10	100	300	500	1000	10,000	100,000	∞
0.50	0.70084	0.94198	1.00988	1.06722	1.12443	1.12890	1.12980	1.13047	1.13108	1.13114	1.13115
0.60	0.73929	0.97453	1.03861	1.09201	1.14465	1.14874	1.14956	1.15018	1.15074	1.15079	1.15080
0.70	0.77758	1.00671	1.06719	1.11696	1.16547	1.16922	1.16997	1.17053	1.17104	1.17109	1.17110
0.80	0.81581	1.03892	1.09607	1.14256	1.18741	1.19085	1.19154	1.19206	1.19253	1.19257	1.19258
0.90	0.85406	1.07142	1.12555	1.16913	1.21077	1.21395	1.21459	1.21507	1.21550	1.21554	1.21555
1.00	0.89240	1.10438	1.15582	1.19683	1.23569	1.23864	1.23924	1.23968	1.24008	1.24012	1.24013

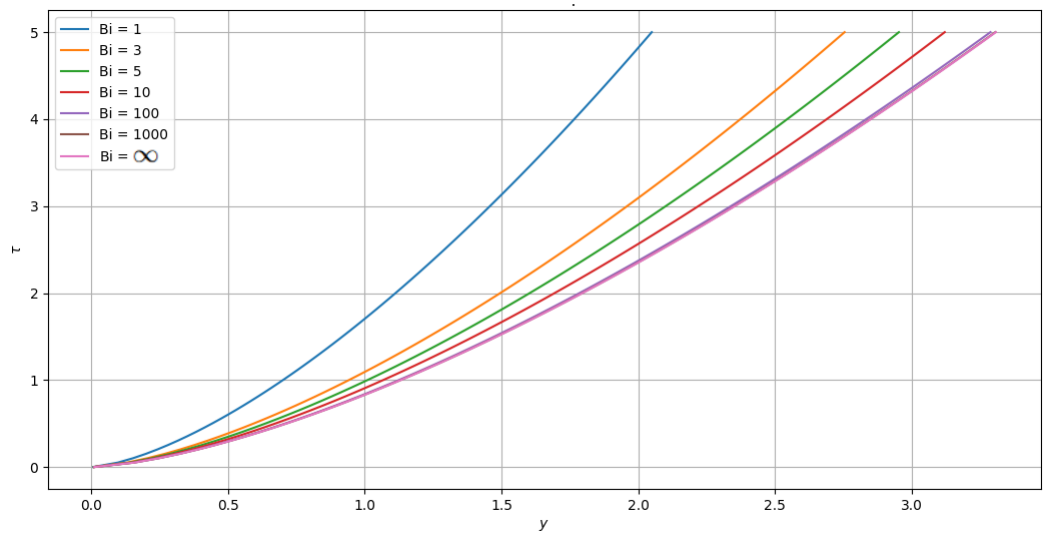

Figure 4. Influence of the Biot number Bi on the dynamics of the free boundary $y = \xi(\tau)$ over time for fixed $\alpha = 0.5$ and $Ste = 1$. The plot corresponding to $\mathrm{Bi} = \infty$ represents the limiting case with a Dirichlet boundary condition at the fixed face.

4.3.4. Some Comments on the Variation of the Characteristic Length

As mentioned at the beginning of this section, the proposed method does not prescribe a fixed value for the characteristic position in advance, since the model corresponds to a semi-infinite domain. For this reason, we present in Figures 5 and 6 the plots of the interface evolution for the dimensionless case, as well as for the recovered physical solution, in which it can be clearly observed that the qualitative behavior of these solutions does not depend on x_0.

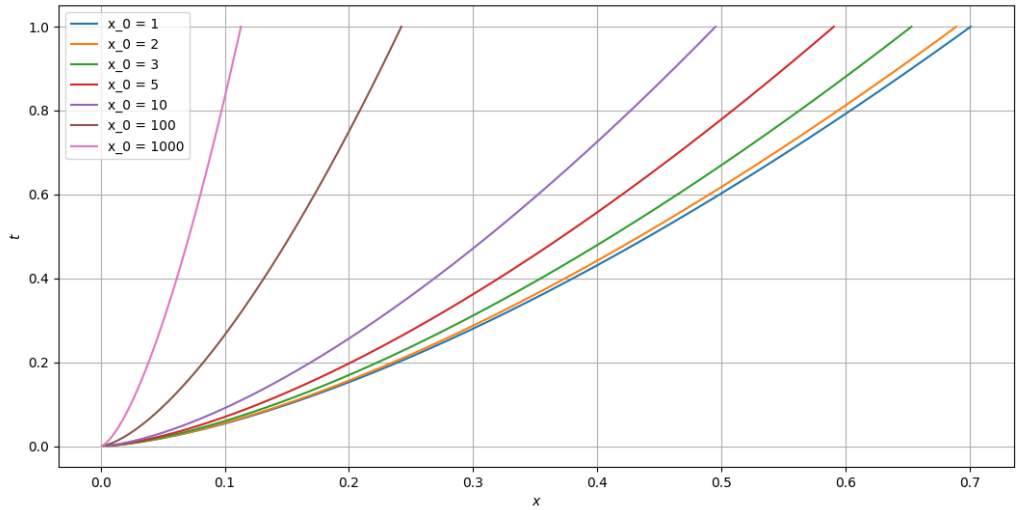

Figure 5. Visualization of the advance of the free boundary $x = s(t)$ for different characteristic lengths.

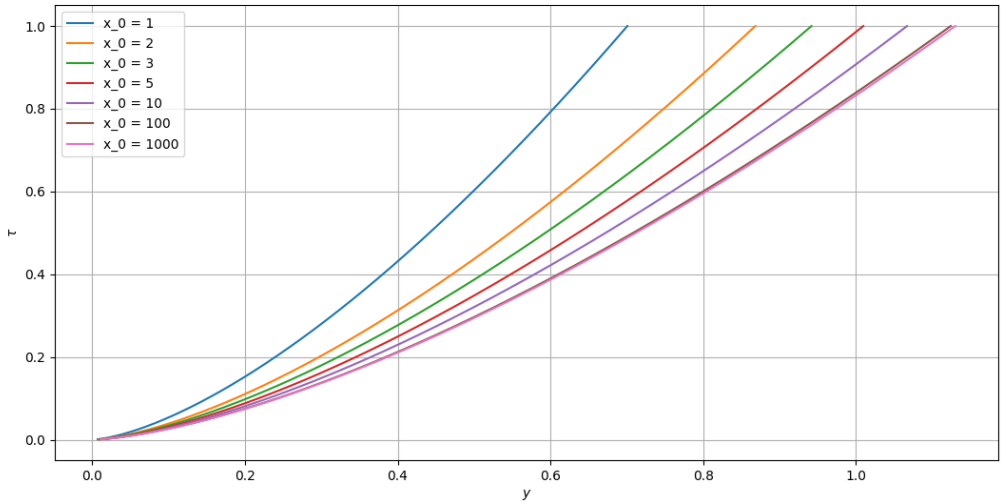

Figure 6. Visualization of the advance of the free boundary $y = \xi(\tau)$ for different characteristic lengths.

4.3.5. Experimental Results

The numerical values of δ_α reported in Tables 3 and 5 suggest that the influence of the Biot number and the Stefan number in the fractional Stefan problem remains qualitatively analogous to that observed in the classical case. For fixed α, an increase in the Stefan number Ste yields a larger free boundary position, reflecting enhanced phase-change progression driven by sensible heat. Similarly, for fixed α, increasing the Biot number Bi produces a progressive growth in δ_α, consistent with more efficient heat transfer at the boundary. In the limit $\text{Ste} \to 0$, the free boundary becomes stationary; consequently, no phase transition occurs and the temperature remains constant. Conversely, when $\text{Bi} \to \infty$, the boundary behaves as if maintained at a prescribed temperature, effectively imposing a Dirichlet condition. In this regime, heat exchange with the environment is instantaneous, and the boundary temperature is directly enforced.

These results are in agreement with classical Stefan-type models and confirm that, although the fractional formulation introduces spatial nonlocality, the roles of Bi and Ste as governing parameters are preserved within the fractional framework.

For the case $\text{Bi} \to \infty$, the boundary behaves as if it were maintained at a constant temperature, effectively imposing a Dirichlet condition. In this limit, the heat transfer between the environment and the material becomes instantaneous, allowing the boundary temperature to be imposed directly. This behavior is consistent with classical Stefan-type models and confirms that, although the fractional formulation introduces nonlocality in space, the functional role of Bi and Ste as governing parameters is preserved within the fractional framework.

5. Conclusions

We have considered a one-dimensional, one-phase fractional Stefan problem with a convective-type boundary condition, derived from a non-Fourier flux expressed through a Caputo fractional derivative. An explicit self-similar solution was obtained in terms of the three-parameter Mittag–Leffler function, which generalizes the classical exponential kernel.

By introducing a dimensionless reformulation of the problem, we highlighted the role of the Stefan number (Ste) and the Biot number (Bi) as key physical parameters. Based on this formulation, we developed computational algorithms to determine both the temperature function and the coefficient characterizing the free boundary. We analyzed the limiting behavior of the model when $\text{Ste} \to 0$ and $\text{Bi} \to 0$, recovering the degenerate cases

of a stationary interface (Ste = 0) and a purely insulating boundary (Bi = 0), respectively. In contrast, as Bi $\to \infty$, we recover the solution to the problem under a Dirichlet condition.

The results confirm that the fractional model retains the essential qualitative features of the classical Stefan problem, while also extending its applicability to systems exhibiting anomalous diffusion and spatial nonlocality. In particular, the influence of the Biot and Stefan numbers within the fractional framework mirrors their classical behavior, thereby preserving their interpretability and usefulness as governing parameters.

As a final contribution, we have constructed an analytical–numerical implementation of the solution using `Python`, enabling efficient evaluation of the free boundary and temperature profiles for various parameter regimes. This tool may serve as a basis for further applications in physical contexts where convective boundaries and anomalous transport mechanisms are relevant. The full implementation is available on Zenodo [16].

Author Contributions: Conceptualization, Mathematical Analysis, and Writing, D.E.G., S.D.R., L.D.V. and D.A.T.; Numerical Methods, D.E.G. and L.D.V. All authors have read and agreed to the published version of the manuscript.

Funding: D.G., S.R., and L.V. were supported by the projects PIP N° 11220220100532 from CONICET and 80020230300102UR from UNR. D.T. was supported by Proyecto Austral N° 006-25CI2002 and S.R. and L.V. by Proyecto Austral N° 006-25CI2001 from Universidad Austral.

Data Availability Statement: The original contributions presented in this study are included in the article. Further inquiries can be directed to the corresponding author.

Conflicts of Interest: The authors declare no conflicts of interest.

References

1. del Teso, F.; Endal, J.; Vázquez, J.L. The one-phase fractional Stefan problem. *Math. Models Methods Appl. Sci.* **2021**, *31*, 83–131.
2. Voller, V.R. Fractional Stefan problems. *Int. J. Heat Mass Transf.* **2014**, *74*, 269–277. [CrossRef]
3. Chugunov, V.; Fomin, S. Application of Fractional Differential Equations for Modeling Bacteria Migration in Porous Medium. *Mathematics* **2024**, *12*, 685. [CrossRef]
4. Hilfer, R. *Applications of Fractional Calculus in Physics*; World Scientific Publishing Company: Singapore, 2000.
5. Liu, F.; Yang, G.C. Rapid solidification of highly undercooled bulk liquid superalloy: Recent developments, future directions. *Int. Mater. Rev.* **2006**, *51*, 145–170. [CrossRef]
6. Mainardi, F. Why the Mittag-Leffler Function Can Be Considered the Queen Function of the Fractional Calculus? *Entropy* **2020**, *22*, 1359. [CrossRef]
7. Suzuki, A.; Fomin, S.; Chugunov, V.; Hashida, T. Mathematical Modeling of Non-Fickian Diffusional Mass Exchange of Radioactive Contaminants in Geological Disposal Formations. *Water* **2018**, *10*, 123. [CrossRef]
8. Vázquez, L.; Trujillo, J.; Velasco, M. Fractional heat equation and the second law of thermodynamics. *Fract. Calc. Appl. Anal. JCR* **2011**, *14*, 334–342.
9. Voller, V.R. Chapter Six-Anomalous Heat Transfer: Examples, Fundamentals, and Fractional Calculus Models. In *Advances in Heat Transfer*; Elsevier: Amsterdam, The Netherlands, 2018; Volume 50, pp. 333–380. [CrossRef]
10. Juric, D.; Tryggvason, G. A Front-Tracking Method for Dendritic Solidification. *J. Comput. Phys.* **1996**, *123*, 127–148. [CrossRef]
11. Gruber, C.; Vogl, C.; Miksis, M.; Davis, S. Anomalous diffusion models in the presence of a moving interface. *Interfaces Free. Boundaries* **2013**, *15*, 181–202. [CrossRef]
12. Voller, V.R. On a fractional derivative form of the Green–Ampt infiltration model. *Adv. Water Resour.* **2011**, *34*, 257–262. [CrossRef]
13. Roscani, S.; Bollati, J.; Tarzia, D. A New Mathematical Formulation for a Phase Change Problem with a Memory Flux. *Chaos Solitons Fractals* **2018**, *116*, 340–347.
14. Kubica, A.; Ryszewska, K. A self-similar solution to time-fractional Stefan problem. *Math. Methods Appl. Sci.* **2021**, *44*, 4245–4275. [CrossRef]
15. Roscani, S.D.; Tarzia, D.A.; Venturato, L.D. The similarity method and explicit solutions for the fractional space one-phase Stefan problems. *Fract. Calc. Appl. Anal.* **2022**, *25*, 995–20220. [CrossRef]
16. Guevara, D.; Venturato, L. Fractional Stefan Problem with Convective Boundary Condition: Python Implementation. 2025. Available online: https://zenodo.org/records/16373258 (accessed on 4 October 2025).

17. Tarzia, D.A. Relationship Between Neumann Solutions for Two-Phase Lame-Clapeyron-Stefan with convective and temperature boundary conditions. *Therm. Sci.* **2017**, *21*, 187–197. [CrossRef]
18. Kilbas, A.; Srivastava, H.; Trujillo, J. *Theory and Applications of Fractional Differential Equations*; Elsevier Science Inc.: Amsterdam, The Netherlands, 2006; Volume 204.
19. Kilbas, A.A.; Saigo, M. On Mittag-Leffler type function, fractional calculus operators and solutions of integral equations. *Integral Transform. Spec. Funct.* **1996**, *4*, 355–370. [CrossRef]
20. Namba, T.; Rybka, P.; Sato, S. Special solutions to the space fractional diffusion problem. *Fract. Calc. Appl. Anal.* **2022**, *25*, 2139–2165. [CrossRef]
21. Roscani, S., Ryszewska, K., Venturato, L.: A One-Phase Space-Fractional Stefan Problem With No Liquid Initial Domain. *SIAM J. Math. Anal.* **2022**, *54*, 5489–5523. [CrossRef]
22. Ryszewska, K. A space-fractional Stefan problem. *Nonlinear Anal.* **2020**, *199*, 112027. [CrossRef]
23. Caruso, N.; Roscani, S.; Venturato, L.; Voller, V. On the Computation of the Prefactor of the Free Boundary in One Dimensional One-Phase Fractional Stefan Problems. *Fractal Fract.* **2025**, *9*, 397. [CrossRef]
24. Gautschi, W. Some Elementary Inequalities Relating to the Gamma and Incomplete Gamma Function. *J. Math. Phys.* **1959**, *38*, 77–81. [CrossRef]
25. Ziegler, F. The multiple meanings of the Stefan-number (and relatives) in refrigeration. *Int. J. Refrig.* **2010**, *33*, 1343–1349. [CrossRef]
26. Solomon, A.D.; Alexiades, V.; Wilson, D.G. The Stefan problem with a convective boundary condition. *Q. Appl. Math.* **1982**, *40*, 203–217. [CrossRef]